ISSN 2635-1676, Nanobiotechnology Reports, 2024, Vol. 19, No. 2, pp. 230–236. © Pleiades Publishing, Ltd., 2024.
Russian Text © The Author(s), 2024, published in Rossiiskie Nanotekhnologii, 2024, Vol. 19, No. 3, pp. 346–353.

NANOMATERIALS FOR FUNCTIONAL AND STRUCTURAL PURPOSES

Technology of Application of the Multilayer Nanofilm ZIF-8/ZIF-67 for CO Detection

M. A. Gritsai[a], V. A. Polyakov[a,*], O. I. Il'in[b], N. N. Rudyk[b], Yu. Yu. Zhityaeva[b], P. V. Medvedev[a,], A. V. Saenko[b], and M. A. Soldatov[a]**

[a] *Smart Materials Research Institute, Southern Federal University, Rostov-on-Don, Russia*
[b] *Institute of Nanotechnologies, Electronics, and Instrumentation Technology, Southern Federal University, Taganrog, Russia*
**e-mail: v.polakov93@gmail.com*
***e-mail: pmedvedev@sfedu.ru*

Received December 7, 2023; revised December 26, 2023; accepted December 26, 2023

Abstract—The process of the formation of gas-sensitive nanofilms ZIF-8 and ZIF-67 on substrates, which are glass chips with contact tracks formed on them, is studied. Multilayer ZIF-8/ZIF-67 nanofilms are grown on a substrate by cyclic layer-by-layer coating in solution. The film growth process is monitored after each cycle using X-ray diffraction, elemental analysis, and scanning electron microscopy. It is shown that at least three 30-minute growth cycles are required to form a strong, uniform ZIF-8 film. Additionally, the sensory properties of the obtained samples for the detection of carbon monoxide CO are studied.

DOI: 10.1134/S263516762360133X

INTRODUCTION

Metal-organic coordination polymers (**MOCP**) consist of metal clusters are connected by bridging organic molecules (linkers) into a three-dimensional framework penetrated by pores and channels, as a result of which they have an exceptionally large specific surface area, ultra-high microporosity, and therefore have excellent sorption capacity [1]. In addition, by varying the size and functionalization of the linker, the pore size can be finely tuned, increasing or decreasing the selectivity of the sorption of certain molecules. Other advantages of MOCP are high thermal and chemical stability, which significantly expands the scope of application of these materials. We note that MOCPs are a relatively new class of compounds, so the first works on their use as gas sensors appeared relatively recently [2]. In recent years, gas sensors based on MOCPs have been an actively developing field in which breakthroughs in increasing the sensitivity, selectivity, energy efficiency, and miniaturization of sensor devices can be expected in the near future. Thanks to the high specific surface area (over 1000 m^2/g) and the ability to fine-tune the selectivity and pore size by varying the structure, MOCPs open up almost unlimited possibilities for creating nanoscale energy-efficient gas sensors for stationary and portable electronics. Promising materials based on MOCPs with luminescent [3–5], chemiresistive [6–8], magnetic [3, 9, 10], and ferroelectric [11–13] mechanisms were considered.Metal-organic coordination polymers of the family **ZIF** (Zeolitic Imidazolate Frameworks) represent a promising class of MOCPs that are topologically isomorphic to natural aluminosilicate minerals, i.e., zeolites. They consist of metal ions ($M = Cd^{2+}$, Cu^{2+}, Co^{2+}, Zn^{2+}), imidazole linkers tetrahedrally coordinated by nitrogen atoms (**Him**), and have a simplified formula $M(Im)_2$. Linkers with metals form bridges with an angle $M–Im–M$, close to 145°, coinciding with the Si–O–Si angle, which is preferred and found in zeolites [14]. This leads to the formation of zeolite-like structures of various topologies. Such frameworks, unlike traditional organometallic compounds, have high chemical stability in boiling organic solvents, water, and alkaline solutions, which is probably due to the high stability of Zn–N bonds for N-donor ligands on the scale of metal-complex formation constants, as well as the hydrophobicity of the pore surface [15].

Among more than 30 described ZIFs, the most studied structure is ZIF-8 [14, 16]. This coordination polymer is composed of Zn^{2+} ions, tetrahedrally coordinated by nitrogen atoms of the imidazole ring of 2-methylimidazole, and has a sodalite topology. Zn^{2+} ions in the ZIF-8 lattice can be partially or completely isomorphically replaced by Co^{2+} ions due to the proximity of their ionic radii, which gives the materials new properties without changing the topology of the framework. A material similar to ZIF-8 containing only cobalt is referred to in publications as ZIF-67. In [17], the high sensitivity of a sensor based on ZIF-67 to

Table 1. Film composition relative to ZIF-8/ZIF-67 application cycles

Sample	Number of cycles	Film composition
S1	5	5 cycles ZIF-8
S2	7	3 cycles ZIF-8 + 2 (1 cycle ZIF-67 + 1 cycle ZIF-8)*

*Film S2 was formed by a series of 30-min layer-formation cycles from ZIF-8 and ZIF-67 precursors. The layers were applied in the following order: ZIF-8, ZIF-8, ZIF-8, ZIF-67, ZIF-8, ZIF-67, ZIF-8.

formaldehyde (5 ppm at 150°C) is shown. In [18] a chemoresistive gas sensor based on ZIF-8/ZIF-67 nanocrystals capable of detecting 10 ppm of toluene, ethanol, carbon monoxide, hydrogen, and nitrogen dioxide is reported. To create simple and effective gas sensors, it is necessary to develop a method for the controlled and reproducible deposition of a dense, uniform layer (film) of ZIF-8/ZIF-67, firmly bonded to the substrate material.

In this work, the dynamics of the cyclic deposition of ZIF-8 layers on the surface of glass chips was studied in order to obtain a uniform MOCP layer on the surface of the glass chip. A sample coated with ZIF-8 only and a sample with varying layers of ZIF-8 and ZIF-67 were obtained. The capacitive sensitivity to CO of the resulting sensors with different layer compositions was assessed.

MATERIALS AND METHODS

Zinc nitrate hexahydrate (99% purity), cobalt(II) nitrate hexahydrate (99%), 2-methylimidazole (**2-mHIm**) (99%), hexane, and methanol were purchased from Sigma Aldrich (USA) and used without additional purification. Deionized water (class A) with a resistivity of 18 MΩ cm was obtained using a Simplicity UV unit (Millipore) (Merck, Germany) from distilled water with a resistivity of 10 MΩ cm.

Synthetic air (N_2 (80%) + O_2 (20%)) was used as the dilution gas. The initial CO concentration was 60 ppm.

Synthesis of ZIF-8/ZIF-67 nanofilms. ZIF films were grown on the surface of a quartz glass substrate, onto which three-layer Cr(15 nm)/Cu(100 nm)/Cr(15 nm) metal contacts with an interdigitated architecture were deposited using magnetron sputtering according to a previously described technique [19]. To degrease the surface of the chip, it was immersed in hexane and treated with ultrasound for 10 min. The chip was then air dried, washed with acetone, and dried again. After this, the chips were immersed for 30 min in a solution prepared by mixing 10 mL of a 25 mM solution of zinc or cobalt(II) nitrate in methanol and 10 mL of a 50 mM solution of 2-methylimidazole in methanol. The interaction of precursors proceeds according to the scheme

$$M(NO_3)_2 + 2(2\text{-mHIm}) \rightarrow M(2\text{-mIm})_2 + 2HNO_3,$$

where $M = Zn^{2+}$, Co^{2+}.

Then the chips were removed from the solution, washed with pure methanol, dried and examined by the methods of X-ray diffraction (**XRD**), X-ray fluorescence analysis (**XRFA**), and scanning electron microscopy (**SEM**).

One stage of immersing the chip in the solution for 30 min corresponded to one cycle of film deposition. Then the chips were used in new cycles in accordance with the data in Table 1. After all deposition cycles were completed, the chip was washed again with methanol and dried at 60°C.

Characterization. The X-ray diffraction profiles were obtained on a D2 PHASER diffractometer (Bruker, USA) in the Bragg–Brentano geometry (CuK_α-radiation, λ = 1.5406 Å). Data were collected over a range of 2θ angles from 5° to 90° with a step size of 0.02° and a data acquisition time of 0.1 s. XRFA was carried out on an M4 Tornado spectrometer (Bruker, USA) equipped with an XFlash 430 detector in the range from 0 to 24 keV. Infrared (IR) spectra were obtained on a Vertex 70 spectrometer (Bruker, USA) in the ATR (attenuated total reflectance) geometry using an MCT detector and a Bruker Platinum ATR attachment. The spectra were measured in the range from 5000 to 30 cm^{-1} with a resolution of 1 cm^{-1} and 64 scans. The comparison sample was air. The geometric parameters and topology of the ZIF films were measured using a Nova NanoLab 600 scanning electron microscope (FEI, the Netherlands) with an accelerating voltage of 10 kV. The capacitance characteristics of the sensor were studied using an E4980A impedance meter (Agilent, USA) at a frequency of 100 Hz at a voltage of 1 V. During the measurements, statistical data was accumulated to obtain the median capacitance value based on the results of 10 measurements. Gas measurements were carried out on a specialized Microgas-FM installation (ZAO Intera, Russia), which allows the mixing flows of diluent and target gas in ratios up to 100 : 1.

The sensitivity of the sensor was measured by the relative change in the capacitance (S_C):

$$S_C = \frac{\Delta C_g}{C_a} \times 100\%,$$

where C_g is the change in the sensor capacity when exposed to a target gas of a certain concentration, and C_a is the capacitance value in the background air atmosphere.

RESULTS AND DISCUSSION

The glass surface acts as a center for the formation of crystallites, coordinating metal ions on itself. The film-formation process is influenced by the concentration of reagents, the diffusion rate, the time of con-

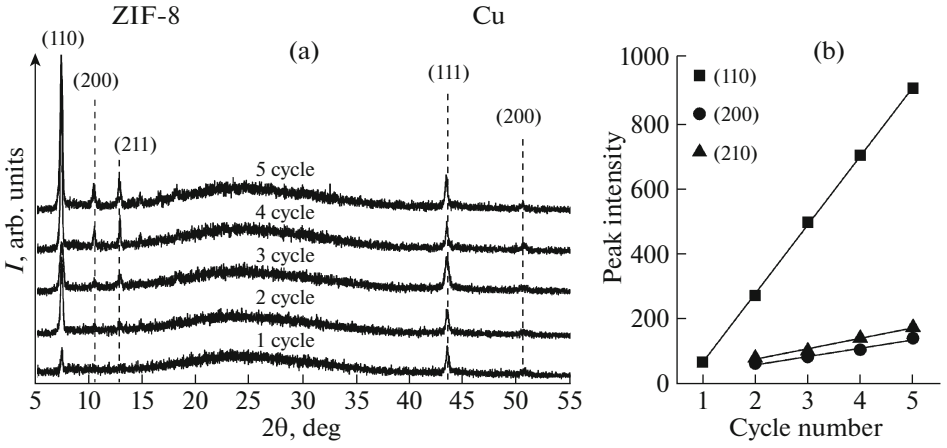

Fig. 1. X-ray diffraction profiles of sample S1 after each film-deposition cycle (a); dependence of the intensity of reflections (110), (200), and (211) on the number of cycles (b).

tact of the matrix with the solution, and the type of solvent. To prevent the rapid precipitation of ZIF-8/ZIF-67 from the solution volume, it is necessary to reduce the reaction rate. For this purpose, low concentrations of reagents were used, and low-polar methanol was used as a solvent, which limits the dissociation of zinc and copper nitrates. As a result, a colloidal solution was formed, allowing reagents to be slowly delivered to the surface of the chip by diffusion. The ZIF-8 formed as a result of the reaction evenly covered its entire surface.

XRD. The growth dynamics of the ZIF-8 film were monitored by X-ray diffraction measurements after each deposition cycle (Fig. 1).

Three characteristic areas can be distinguished on the radiographs. In the 2θ range from 5° to 24° there is a region characteristic of the ZIF-8 phase. From 15° to 40° from the substrate, a low-intensity broad peak can be observed, corresponding to the amorphous structure of SiO_2 glass [20]. Finally, from 42° to 57°, peaks (111) and (200) are observed, characteristic of contact tracks of metallic copper [21]. The absence of a change in the intensity and width of the copper peaks indicates that during film deposition, the metal of the contact tracks is not destroyed under the influence of reagents. Also, no noticeable peaks characteristic of chromium metal were observed [22], probably due to its relatively thin layer and background noise caused by the amorphous glass. Changes are observed only in the ZIF-8 reflection region. After the first cycle of film deposition, a low-intensity reflection (110) at 7.5° is observed, which is characteristic of the ZIF-8 crystalline phase [14]. An increase in the number of film-growth cycles leads to a steady increase in the intensity of this reflection (Fig. 1b). Starting from the second cycle, reflections of the (200) and (211) planes appear at angles of 10.7° and 13°, respectively, and starting from the third cycle, additional peaks were observed at 15°, 16.7°, and 18.3°, which is consistent with published data. The increase in the intensity of these reflections is also monotonous, but less intense than in the case of (110). This fact indicates a predominantly ordered orientation of ZIF-8 crystals during film growth.

X-ray fluorescence analysis in accordance with X-ray diffraction data showed a steady increase in the zinc content with an increase in the number of film-growth cycles (Fig. 2a).

Data collection points were selected at 10 random sites for the first (Fig. 2b) and last cycle (Fig. 2c). Microfocus XRF with a spatial resolution of ~15 μm was used to monitor the uniformity of the distribution of elements in the film with local sensitivity. In particular, the thickness of the ZIF-8 film on the electrodes and the glass surface was compared after five deposition cycles. The measurement results confirmed the uniformity of the films over the entire surface of the chips. Figures 2b and 2c show the opalescent white coating and changes in the layer thickness after five cycles.

Scanning electron microscopy. SEM examination was carried out after each coating cycle. After the first cycle, predominantly individual crystals with sizes from 100 to 300 nm with a rhombic dodecahedral [23], and also the spherical shape characteristic of ZIF-8 were observed on the chip surface (Fig. 3).

In some areas, crystals located quite close to each other began to merge into agglomerates. The process of combining crystals into a film is most pronounced in the second cycle, and at the end of the third, individual crystals disappear and a homogeneous film is formed. In subsequent cycles, the film continues to grow. The appearance of cracks on the surface is associated with the effect of an electron beam during SEM examination. Thus, it was found that a minimum of three 30-min deposition cycles are required to form a homogeneous ZIF-8 film.

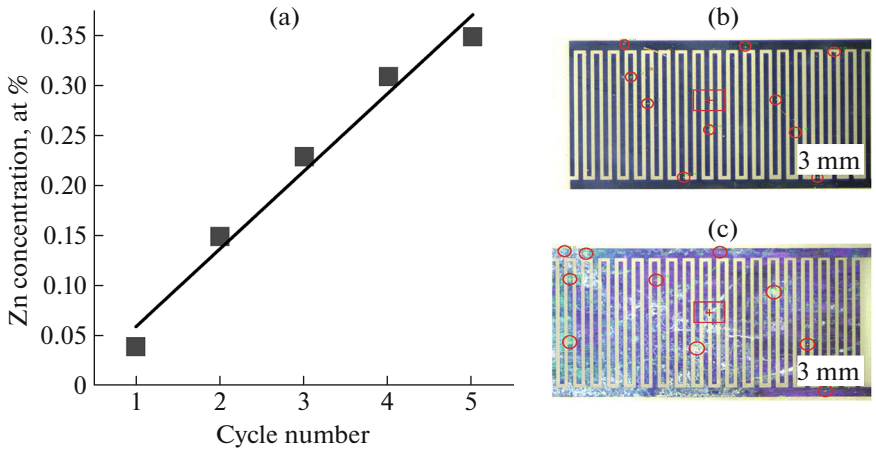

Fig. 2. Dependence of the zinc content on the number of film-deposition cycles (a); images of the chip after one (b) and five cycles (c). Circles indicate locations where elemental-analysis data were collected.

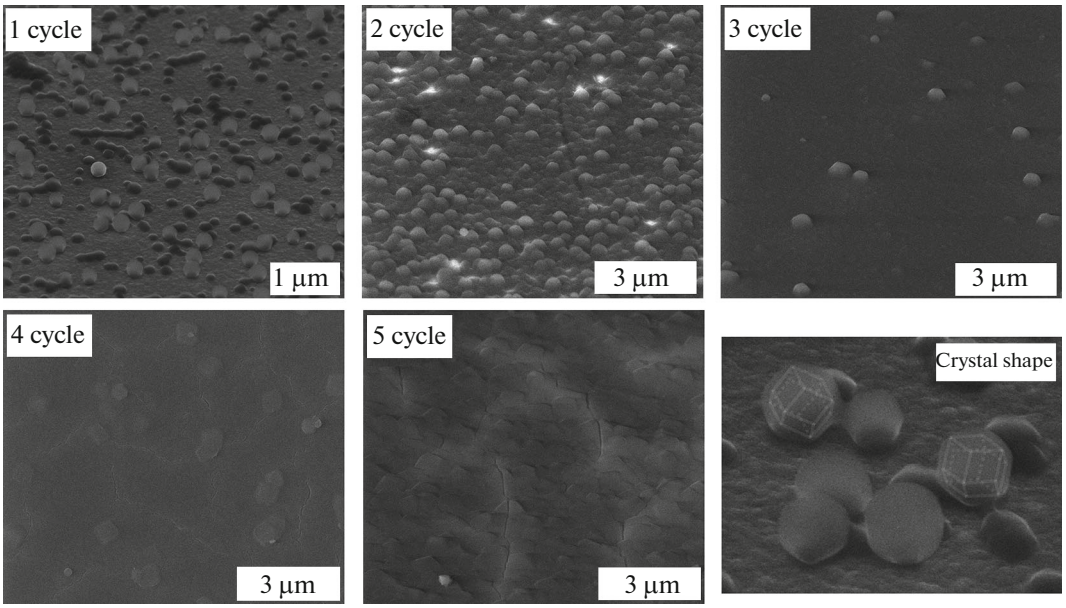

Fig. 3. SEM images of the chip surface obtained after each deposition cycle.

IR spectroscopy. Since ZIF-8 has zinc ions bound to 2-methylimidazole molecules, the IR spectrum of pure ZIF-8 should be similar to that of the pure linker. Figure 4 shows the comparative IR spectrum of pure glass, the linker, and two regions of the chip after five deposition cycles: a region containing the conductive-path metal and the region without metal.

The spectra of these two areas with the ZIF-8 film differ slightly. Thus, the region without a conductive path has a wide peak in the range of 965–815 cm^{-1}, corresponding to vibrations of Si–OH bonds in glass [24]. There are no other differences between them, so all further considerations are valid for both spectra. The frequencies 670 and 760 cm^{-1} can be attributed to bending vibrations of the C–H bonds of the aromatic ring [25]. Oscillations at 950 cm^{-1} characterize the combined contribution of stretching vibrations of C–N bonds and bending vibrations of C–H of the methyl group of 2-methylimidazole, while the next peak at 990 cm^{-1} is caused only by bending vibrations of the methyl group [26]. The absorption peaks at 1144 and 1180 cm^{-1} refer to stretching vibrations of C–N bonds [37], and the peak at 1310 cm^{-1} characteristic of deformation vibrations of C–N bonds [27]. The absorption bands at 1144 and 1180 cm^{-1} shifted relative to those in the pure linker due to the coordination of amino groups by zinc. The oscillation range from 1500 to 1320 cm^{-1} (the area highlighted by a rectangle in the

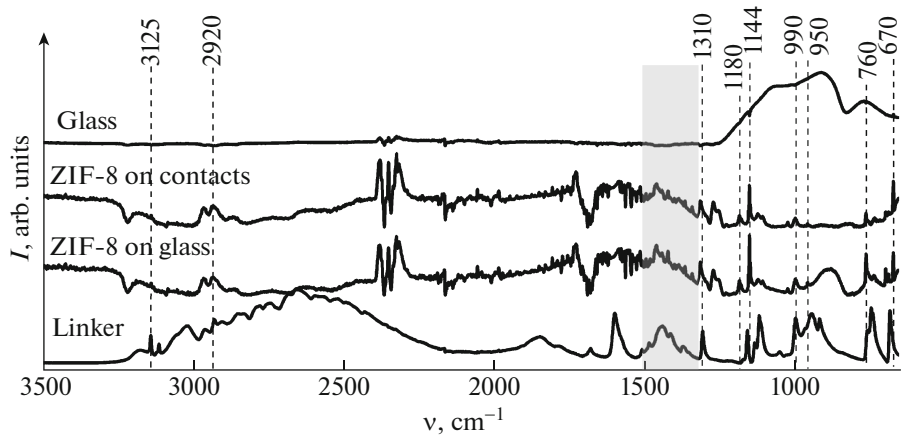

Fig. 4. IR spectra of the chip after five coating cycles compared to the spectrum of the substrate and linker.

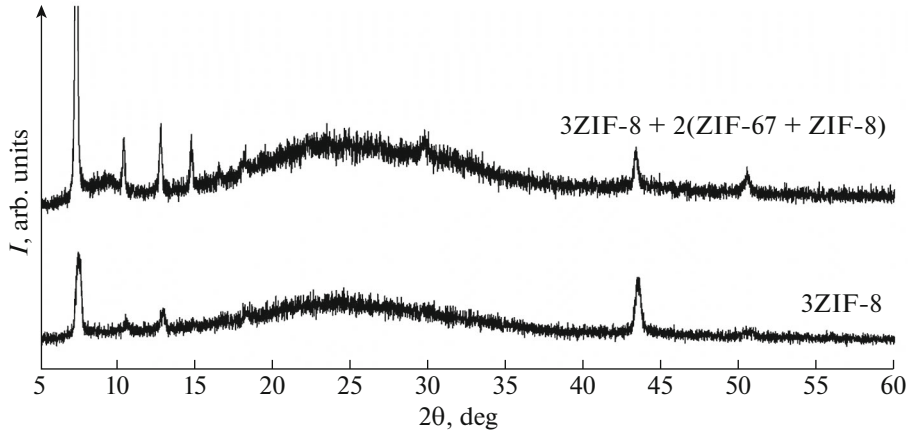

Fig. 5. X-ray diffraction profiles of sample S2 after the third and seventh cycles of ZIF-8/ZIF-67 deposition.

figure) corresponds to bending vibrations of the imidazole ring [25]. The absorption bands 3125 and 2920 cm^{-1} can be attributed to aromatic and aliphatic stretching vibrations of the C–H bonds of the linker, respectively [18]. No other vibrations were detected, which confirms the chemical purity of the resulting film.

Functionalization of films with cobalt. In order to increase the sensitivity and subsequent detection of CO, functionalized films based on ZIF-8/ZIF-67 were formed. Due to the close values of the ionic radii, as well as the stable oxidation state +2, Co^{2+} ions can partially or completely replace Zn^{2+} ions in the lattice. When completely replaced, a ZIF-67 structure similar to ZIF-8 is formed. However, it was found that ZIF-67 is not able to form a film on the surface of a quartz glass substrate with conductive paths, but is able to grow on an existing ZIF-8 layer. This may be due to the less strong bond of cobalt ions with the surface of the substrate, as well as the greater affinity of ZIF-67 for ZIF-8 than for quartz glass or metal. Therefore, after three cycles of ZIF-8 coating, we also tried to apply layers of ZIF-67, alternating them with layers of ZIF-8. The color of the ZIF film changed to lilac blue. Figure 5 shows the X-ray diffraction pattern of the resulting sample.

In this case, the appearance of a reflection of the (110) plane and the absence of other reflections were observed, which can be explained by the greater noise of the base line of the diffraction pattern. Elemental analysis showed the presence of cobalt in sample S2. According to the XRF data, the Zn and Co contents were 0.73 and 0.29 at %, respectively. The data obtained correlate with the actual ratio of the number of layers of ZIF-8 (5/7) and ZIF-67 (2/7).

Gas measurements. Experimental studies were carried out on the effect of CO at concentrations from 3 to 30 ppm on changes in the capacitance values of sample S1. Measurements at room temperature did not show changes in the resistance or capacitance, including in an extended frequency range (from 20 Hz to 2 MHz), therefore, to increase the sensitivity of the

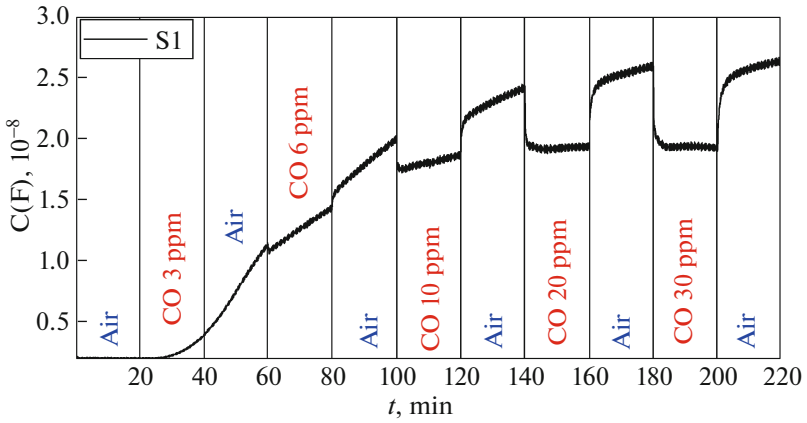

Fig. 6. Histogram of the capacitive sensitivity of sample S1 depending on the measurement frequency.

samples, similar measurements were carried out when the sample was heated to 180°C. An increase in temperature promotes the desorption of atmospheric moisture, freeing the pores of the MOCP for the adsorption of gases and reducing the activation energy. However, in this case, sample S1, containing only ZIF-8, did not show any changes. In order to increase the likelihood of CO molecules overcoming the energy barrier, sample S2 was synthesized, containing both ZIF-8 and ZIF-67 layers. Modification of the film with cobalt(II) ions made it possible to sharply increase its sensitivity (Fig. 6).

At the beginning of the process of supplying low concentration carbon monoxide CO, nonlinearity is observed, which can be explained by the process of filling the porous structure of the MOCP with gas molecules. This leads to an increase in the film capacitance. It was found that heating the sample to 180°C and functionalizing it with cobalt made it possible not only to initiate the sensitivity of the sensor to CO, but also to reduce the noise level during measurements. Based on the processing of the collected data, histograms of the capacitive sensitivity of sample S2 to various CO concentrations were constructed (Fig. 7).

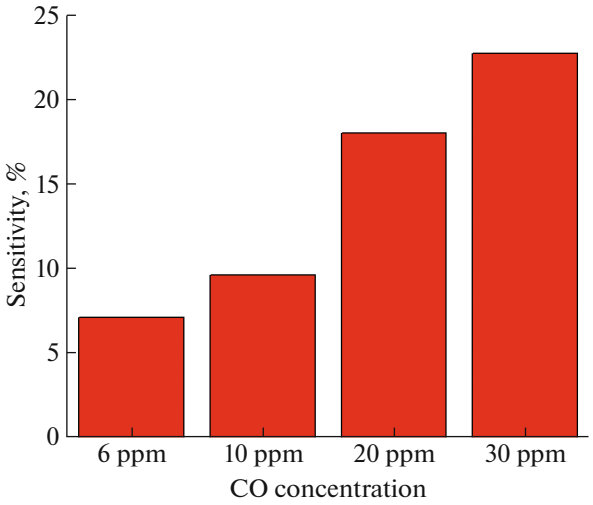

Fig. 7. Histograms of the S_C capacitive sensitivity of sample S2 to different CO concentrations.

Sample S2 showed a high sensitivity even at low CO concentrations of 6 ppm ($S_C = 7\%$) and 10 ppm ($S_C = 10\%$).

CONCLUSIONS

Multilayers of ZIF-8/ZIF-67 nanofilms were grown on a glass substrate with an interdigitated electrode structure. The sequential growth of nanofilms was characterized by XRD, XRF, SEM, and IR spectroscopy. The resulting nanofilm containing only ZIF-8 did not exhibit gas sensitivity even with additional heating. Functionalization of the ZIF-8 film with ZIF-67/ZIF-8 multilayer films results in a dramatic increase in sensor sensitivity. It is shown that heating the samples leads to an increase in the capacitance of the structure. At the beginning of the process, when low concentrations of CO are supplied, a nonlinear change in the capacitance characteristics is observed. This effect may be associated with filling of the porous structure of the MOCP with gas molecules, which leads to an increase in the film capacity.

FUNDING

The study was supported by the Russian Science Foundation (grant no. 22-29-01124).

CONFLICT OF INTEREST

The authors of this work declare that they have no conflicts of interest.

REFERENCES

1. O. M. Yaghi, M. O'Keeffe, N. W. Ockwig, et al., Nature **423**, 705 (2003). https://doi.org/10.1038/nature01650
2. S. Achmann, G. Hagen, J. Kita, et al., Sensors **9**, 1574 (2009).
3. A. A. García-Valdivia, S. Pérez-Yáñez, J. A. García, et al., Sci. Rep. **10**, 8843 (2020). https://doi.org/10.1038/s41598-020-65687-6
4. Y. Cui, Y. Yue, G. Qian, and B. Chen, Chem. Rev. **112**, 1126 (2012). https://doi.org/10.1021/cr200101d
5. W. P. Lustig, S. Mukherjee, N. D. Rudd, et al., Chem. Soc. Rev. **46**, 3242 (2017). https://doi.org/10.1039/C6CS00930A
6. L. E. Kreno, J. T. Hupp, and R. P. Van Duyne, Anal. Chem. **82,** 8042 (2010). https://doi.org/10.1021/ac102127p
7. M. K. Smith, K. E. Jensen, P. A. Pivak, and K. A. Mirica, Chem. Mater. **28**, 5264 (2016). https://doi.org/10.1021/acs.chemmater.6b02528
8. M.-S. Yao, J.-J. Zheng, A.-Q. Wu, et al., Angew. Chem. Int. Ed. **59**, 172 (2020). https://doi.org/10.1002/anie.201909096
9. H.-Y. Li, S.-N. Zhao, S.-Q. Zang, and J. Li, Chem. Soc. Rev. **49**, 6364 (2020). https://doi.org/10.1039/C9CS00778D
10. A. Tissot, X. Kesse, S. Giannopoulou, et al., Chem. Commun. **55**, 194 (2019). https://doi.org/10.1039/C8CC07573E
11. J. E. Clements, P. R. Airey, F. Ragon, et al., Inorg. Chem. **57**, 14930 (2018). https://doi.org/10.1021/acs.inorgchem.8b02625
12. W. Zhang and R.-G. Xiong, Chem. Rev. **112**, 1163 (2012). https://doi.org/10.1021/cr200174w
13. W.-J. Xu, P.-F. Li, Y.-Y. Tang, et al., J. Am. Chem. Soc. **139**, 6369 (2017). https://doi.org/10.1021/jacs.7b01334
14. K. S. Park, Z. Ni, A. P. Côté, et al., Proc. Natl. Acad. Sci. USA **103**, 10186 (2006). https://doi.org/10.1073/pnas.0602439103
15. R. J. Sundberg and R. B. Martin, Chem. Rev. **74**, 471 (1974). https://doi.org/10.1021/cr60290a003
16. R. Banerjee, A. Phan, B. Wang, et al., Science **319**, 939 (2008). https://doi.org/10.1126/science.1152516
17. E.-X. Chen, H. Yang, and J. Zhang, Inorg. Chem. **53**, 5411 (2014). https://doi.org/10.1021/ic500474j
18. D. Matatagui, A. Sainz-Vidal, I. Gràcia, et al., Sens. Actuators, B **274**, 601 (2018). https://doi.org/10.1016/j.snb.2018.07.137
19. A. M. Aboraia, A. A. A. Darwish, V. Polyakov, et al., Opt. Mater. **100**, 109648 (2020). https://doi.org/10.1016/j.optmat.2019.109648
20. F. Khamis and E. D. Arafah, Asian J. Phys. Chem. Sci. **3**, 1 (2017). https://doi.org/10.9734/AJOPACS/2017/35542
21. P. Sen, J. Ghosh, A. Abdullah, et al., J. Chem. Sci. **115**, 499 (2003). https://doi.org/10.1007/BF02708241
22. G. Boisselier, F. Maury, and F. Schuster, J. Nanosci. Nanotechnol. **11**, 8289 (2011). https://doi.org/10.1166/jnn.2011.5028
23. V. V. Butova, E. A. Bulanova, V. A. Polyakov, et al., Inorg. Chim. Acta **492**, 18 (2019). https://doi.org/10.1016/j.ica.2019.04.011
24. T. Oh, J. Korean Phys. Soc. **56**, 1150 (2010). https://doi.org/10.3938/jkps.56.1150
25. P. Pillai, S. Dharaskar, S. Sasikumar, and M. Khalid, Appl. Water Sci. **9**, 150 (2019). https://doi.org/10.1007/s13201-019-1030-9
26. A. Di Santo, H. Osiry, E. Reguera, et al., New J. Chem. **42**, 1347 (2018). https://doi.org/10.1039/C7NJ03585C
27. D. Huang, Q. Xin, Y. Ni, et al., RSC Adv. **8**, 6099 (2018). https://doi.org/10.1039/C7RA09794H